Viscoelastic drop falling through a viscous medium

Swarnajay Mukherjee and Kausik Sarkar
Department of Mechanical Engineering, University of Delaware, Delaware 19716, USA

(Received 3 August 2010; accepted 9 December 2010; published online 11 January 2011)

Deformation and sedimentation velocities of a viscoelastic drop falling through a Newtonian medium are numerically investigated using a front-tracking finite difference method. In contrast to a viscous drop, viscoelasticity deforms an initially spherical drop into an oblate shape and decreases its sedimentation velocity. Further increase of elasticity results in a dimple at the rear end, as the viscoelastic stress at the trailing end of the drop pulls the drop interface inward. The dimple becomes more prominent with increasing Deborah number, amount of polymeric viscosity, and capillary number. An approximate analysis is performed to model the stress development along the axis of symmetry, specifically its increase at the rear end that governs the dimple formation. For even higher values of Deborah number, the interfacial tension cannot balance the viscoelastic stresses leading to an unstable situation toward a toroidal shape. We numerically find the critical Deborah number for the transition. It shows an approximate inverse scaling with capillary number. For unstable cases, downward progressing dimple develops a globular end. Development of the globular end results in a sudden increase in the cross-sectional area of the drop and a sharp decrease of the settling velocity. © *2011 American Institute of Physics*. [doi:10.1063/1.3533261]

I. INTRODUCTION

The problem of a falling viscous drop was independently solved in absence of inertia assuming a spherical shape by Hadamard[1] and Rybczynski,[2] providing expressions for its terminal velocity and drag. Later, Taylor and Acrivos[3] theoretically showed that at zero Reynolds and finite capillary numbers, the drop remains exactly spherical,[4,5] and only at finite Reynolds number it assumes an oblate shape. In this paper, we investigate departure from sphericity of a settling viscoelastic drop, stability of its shape, and settling velocity. We also find the critical parameters for transition between a stable and an unstable shape.

In recent years, much effort has been devoted toward understanding viscoelastic effects on particle motion.[6] Creeping motion of a sphere in a viscoelastic fluid has been used as a benchmark problem for testing numerical algorithms of non-Newtonian flows.[7,8] A drop presents additional complexity due to its deformation. The case of a Newtonian drop rising in a viscoelastic media has received a lot of attention and has been associated with a number of unusual phenomena such as a negative wake[9]—the velocity vectors just below the rear end and close to the vertical axis of a rising bubble are in the direction of motion of the bubble, while little further away they are in the opposite direction—or a cusped shape at the trailing end beyond a critical bubble volume.[10,11] The steady state velocity was also found to experience a sudden jump beyond a critical volume.[12] Recently, Pillapakkam *et al.*[13] investigated this problem using a three dimensional finite-element-level set method.

The opposite case of a non-Newtonian drop falling/rising in a Newtonian medium has received much less attention. One of the first studies by Wagner and Slattery[14] modeled both the drop and the surrounding media as third order fluids. They analyzed non-Newtonian and inertial effects as double perturbation using a matched asymptotic expansion to find an expression for the drag force and a prolate shape for a Newtonian drop moving through non-Newtonian medium. Most recently, Sostarecz and Belmonte[15,16] performed a combined experimental and theoretical analysis of a falling polymeric drop. Their experiment showed that a polymer drop assumes an oblate shape or a shape with a dimple at the rear end. The drop may fall with a stable dimple or may become unstable upon increase of drop volume, when the dimple extends to the other side of the drop leading to a toroidal shape. Theoretically, they found the dimple shape of a falling drop, modeling the drop constitutive equation as a simple fluid of order three. Recently, You *et al.*[17] described in detail a finite volume algorithm with FENE-CR (finite extensible non-linear elastic-Chilcott-Rallison) model and body-fitted coordinate system in the axisymmetric geometry, which they then used to compute drop shapes when either of the media is viscoelastic for a set of capillary number, Reynolds number, viscosity ratio, and polymeric content. They found a dimple in the rear end for a viscoelastic drop in a Newtonian medium, which forms an inward cusp for high elasticity and low surface tension. A follow-up study on the effects of confinement found it to induce a cylindrical shape on the drop.[16]

For a viscoelastic drop falling or rising in a Newtonian media, interfacial tension tries to retain the spherical drop shape, while viscoelastic stresses at the rear end pulls the drop surface inward creating a dimple. When the viscoelastic force dominates, the drop becomes unstable giving rise to ultimately a toroidal drop. Here a detailed understanding of this competing dynamics is studied by performing a numerical simulation with systematic variation of the governing parameters. The front-tracking finite difference code has previously been successfully applied to investigate a number of

viscoelastic problems involving drops.[18–23] Because the governing equation and the computational method have been discussed in detail there, we provide only a brief description in Sec. II. Section III describes convergence and domain independence study. Section IV presents the results, and the study is summarized in Sec. V.

II. PROBLEM SETUP

Initially at $t=0$, we place a viscoelastic drop of radius a in a computational domain with wall boundary conditions on four sides (see domain dependence study below) and periodic boundary condition in the vertical direction. The drop satisfies an Oldroyd-B equation, the simplest rate type constitutive equation with a single relaxation time λ. We have carefully checked the numerical accuracy of the method.[19,20,23] Introducing finite extensibility did not qualitatively change the dynamics for the range of Deborah number studied here. The drop has a solvent viscosity μ_{sd} and a polymeric viscosity μ_{pd}, with $\beta=\mu_{pd}/(\mu_{pd}+\mu_{sd})$. The viscosity ratio $\lambda_\mu=\mu_d/\mu_m$ between the drop viscosity $\mu_d=\mu_{pd}+\mu_{sd}$ and the matrix viscosity μ_m is assumed to be unity. The front-tracking finite difference[24] method with viscoelastic implementation has been described in detail in our previous publication.[19,25]

We use drop radius a and $a/\bar{U}$ to nondimensionalize length and time, respectively, where $\bar{U}$ is the velocity scale to be defined below. ρ is the density, Γ is the interfacial tension, and subscripts m and d refer to the matrix and the drop phases. One then obtains governing dimensionless numbers Reynolds number $\mathrm{Re}=\rho_m a\bar{U}/\mu_m$, capillary number $Ca=\bar{U}\mu_m/\Gamma$, $De=\lambda\bar{U}/a$, and Froude number $Fr=\bar{U}/\sqrt{ga}$. Along with the ratios defined above, we also have density ratio $\lambda_\rho=\rho_d/\rho_m$ driving the settling. The value of β is 0.5 for all the computations, except where we study the effect of β variations. In this paper, $\lambda_\rho=7.5$. Note that the explicit nature of the code restricts us [despite the ADI (alternating direction implicit) implementation of the viscous terms] to a small nonzero Reynolds number. Below, we discuss its effects.

III. CONVERGENCE AND DOMAIN DEPENDENCE

Convergence of the algorithm used to simulate fluids with Oldroyd-B constitutive relation for a drop deformation in a shear flow has been established in our previous publications.[19,20,22,23] For the falling drop problem, grid independence is investigated in Fig. 1 where we plot the transient velocity of the falling viscoelastic drop nondimensionalized by U_{HR} for varying discretization levels for $Ca=0.346$, $De=1.73$, and $Fr=0.387$ from $48\times48\times96$ to $129\times129\times258$ in a domain size of $9a\times9a\times18a$. U_{HR}, used to define the nondimensional numbers, is the terminal velocity for a Newtonian drop in a creeping flow given by Hadamard and Rybczinski[1,2]

$$U_{\mathrm{HR}}=\frac{2}{3}\frac{(\rho_d-\rho_m)ga^2}{\mu_m}\left(\frac{1+\lambda_\mu}{2+3\lambda_\mu}\right). \tag{1}$$

The transients are almost the same above $89\times89\times178$. In the inset we plot the percentage relative error with respect to the finest grid as a function of the inverse square of the resolution $1/(\Delta x)^2[=(n_x/L_x)^2]$ to note a quadratic convergence. n_x and Δ_x are the number of grid points and grid spacing in the x-direction. We choose $89\times89\times178$ for this domain size as our level of resolution where the steady state value shows an error less than 1.5%.

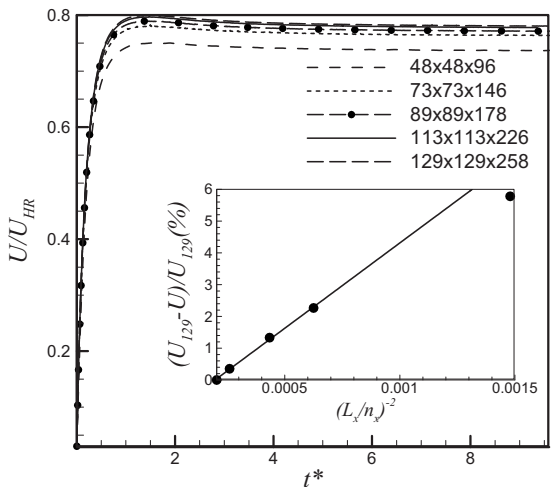

FIG. 1. Convergence of terminal velocity of a falling viscoelastic drop using different grid resolution for $Ca=0.346$, $De=1.73$, and $Fr=0.387$. Inset shows the relative percentage error with respect to the finest grid.

To study the effect of domain size, in Fig. 2 we plot the velocity of a falling viscoelastic drop for the same parameters ($Ca=0.346$ $De=1.73$, $Fr=0.387$) for a set of domain heights (h) keeping the cross-section constant at $9a\times9a$. The velocity of a falling drop decreases as the height increases due to decreased interactions with periodic images of the drop. We also plot the relative error (with respect to the domain with the largest h) of the steady state velocity and notice that the error varies linearly with the inverse of domain height and beyond $18a$ the error is around 3%. We choose $18a$ to be our domain height. For investigating the effect of cross-sectional width of the domain, we vary domain cross-section from $6a\times6a$ to $15a\times15a$ in Fig. 2 (the height is kept constant $18a$) again for the same values of the nondimensional numbers. Here, we notice that as the domain is made larger the settling velocity increases. In the inset we plot the relative error as before. We adopt a domain cross-sectional size of $13a\times13a$ where the error is less than 4%. Consequently, we choose $129\times129\times178$ grids in this domain of size $13a\times13a\times18a$.

Note that domain size affects drop velocity,[16] and we settle on a size in the interest of achieving a reasonable computational time. However, while drop velocity decreases with increasing domain height and decreasing cross-section, the effects are exactly the same for both viscous and viscoelastic drops. As a result, when we nondimensionalize drop settling velocity with the corresponding Newtonian value U^* obtained from simulation using the same domain size (instead of U_{HR}), domain size has little effect on the steady state drop velocity as shown in Fig. 3. This makes us reasonably certain that the simulation with the domain size chosen is sufficient to elucidate viscoelastic effects we are interested in. For unstable shapes and transition study below, simulations with

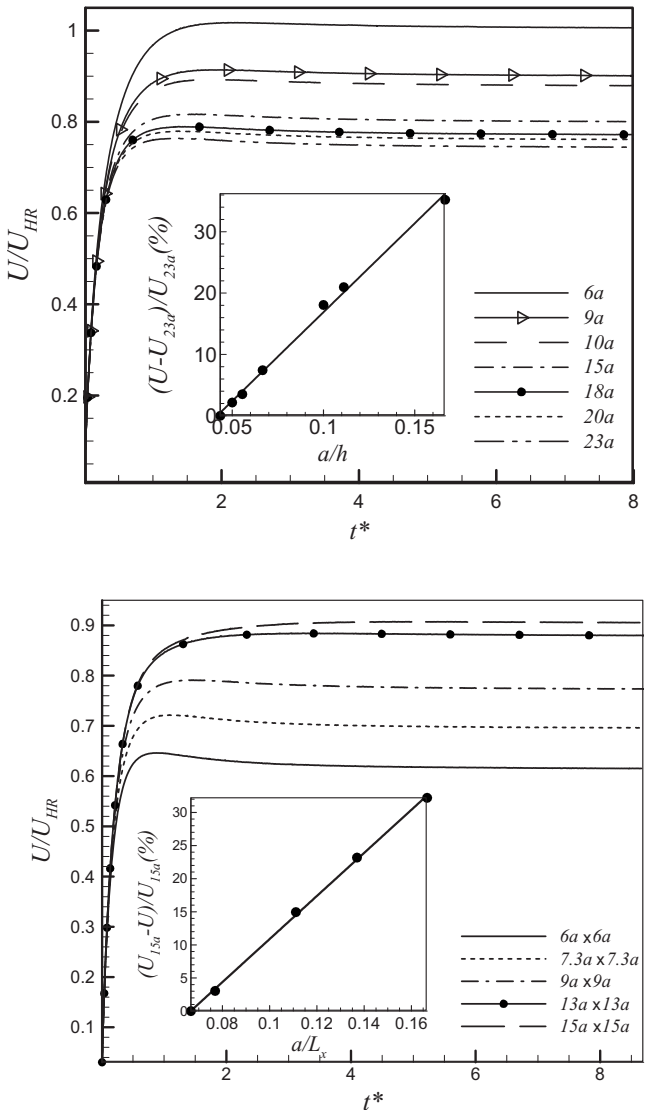

FIG. 2. Domain-size dependence: Terminal velocity of a viscoelastic drop for different domain height h (top) and domain cross-sectional length L_x (bottom) for the same values as in Fig. 1. Their insets show the relative percentage error with respect to the maximum domain height or cross-sectional length.

higher resolutions are also used to ensure accuracy of the results. Note that Pillapakkam *et al.*[13] in their investigation of a rising viscous drop in a viscoelastic medium used two domain sizes of $2\times2\times4$ and $1.5\times1.5\times3$ for bubble radii of 0.125–0.3 commenting that although the presence of walls lowers the bubble rise velocity, the qualitative dependence of the bubble rise velocity on the bubble volume stays the same as the domain sizes are changed. Below we use $\bar{U}=U^*$ for nondimensionalization.

IV. RESULTS

As noted before, a Newtonian drop falling in a Newtonian medium under the assumption of Stokes flow condition remains perfectly spherical for all finite values of capillary number.[3] Inertia changes it into an oblate shape. As we mentioned before, we are restricted to a small value of Reynolds number ($\mathrm{Re}\leq0.1$) due to the explicit nature of the code

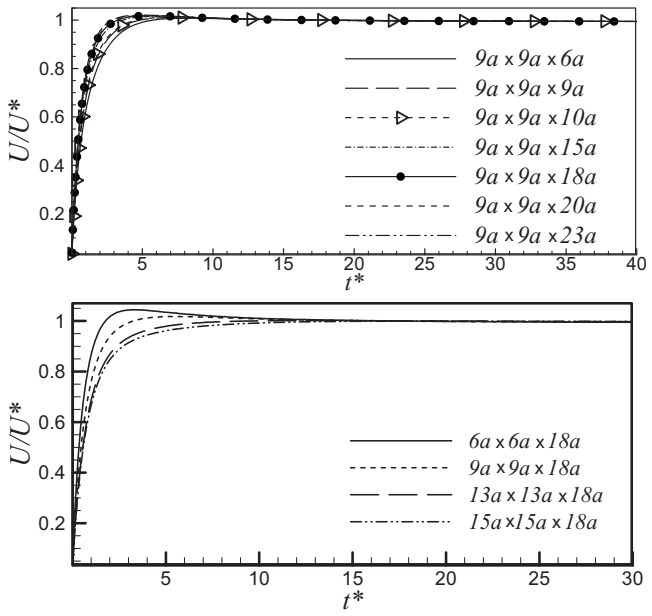

FIG. 3. Velocity of a viscoelastic drop normalized by the corresponding Newtonian value obtained using the same domain for various domain heights (top) and lengths (bottom). The nondimensional numbers are the same as the previous figure.

used. However, the nonspherical drop shapes presented here are not due to inertia but due to drop viscoelasticity. To establish this, we show two shapes of a falling Newtonian drop in a Newtonian medium for two capillary numbers and corresponding velocity vectors in Fig. 4. The drop is spherical with deviation from the sphericity less than 1%, and the velocity field is top-and-bottom symmetric. This leads us to conclude that in our simulation, effects of inertia are negligible.

A. Effects of Deborah number and β variation

When a spherical Oldroyd-B drop is released in a Newtonian liquid of lower density, surface tension tries to maintain a spherical shape, and the viscoelastic stresses developed inside the drop try to deform it. With increasing Deborah number, the drop loses its sphericity and becomes flattened at the rear end.[15]

As the drop deforms, the drag force increases, reducing the falling velocity. In Fig. 5, we plot the transient velocity for different Deborah numbers for $Ca=0.61$. (Although the falling drop velocity is negative, we plot the absolute value of the velocity; drop velocity never changes sign). We

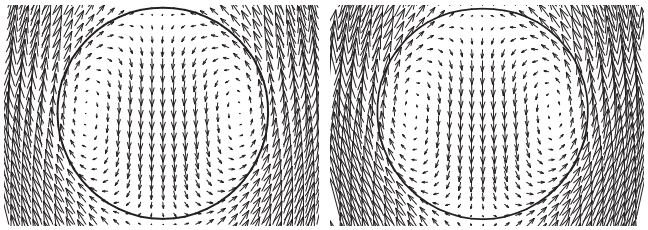

FIG. 4. Drop shapes along with the velocity vectors (with respect to the drop) for falling Newtonian drops at $Ca=0.3$ and $Ca=0.152$ where $Fr=0.34$ for both cases.

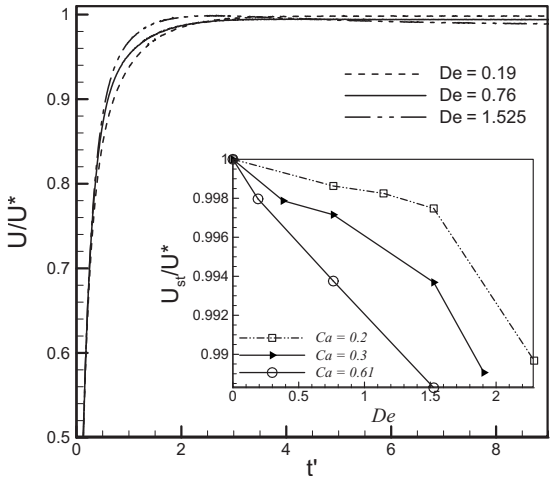

FIG. 5. Effect of Deborah number on the velocity of a falling viscoelastic drop for Ca=0.61 and Fr=0.34. Inset shows the steady state velocity as a function of Deborah number for three capillary numbers.

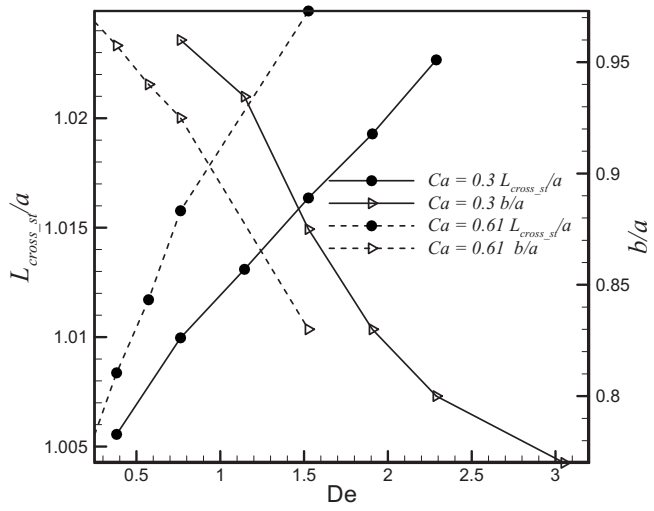

FIG. 7. Steady state L_{cross} and b for two sets of capillary numbers with varying De and Fr=0.34.

observe that an increase in viscoelasticity (higher De) lowers the terminal falling velocity below the Newtonian value. However, viscoelasticity results in an initial increase in the velocity which is due to the fact that during the initial stage, the drop behaves like one with lower viscosity because viscoelastic stresses take time to grow (a drop with lower viscosity would have a higher settling velocity). In a Newtonian system at finite capillary numbers, a drop does not deform in a Stokes flow, and the terminal velocity develops instantaneously. The present simulation is at a small but finite inertia, and the Newtonian case correspondingly reaches its finite value after a very short interval. The steady state values plotted in the inset shows a monotonic decrease in settling velocity with increasing De. In Fig. 6, we study the effects of increasing β, the ratio of polymeric to the total drop viscosity, by increasing the polymeric viscosity and reducing solvent viscosity keeping the total viscosity the same. Increasing β increases the viscoelastic stresses and the flattening of the drop. The velocity consequently decreases, similar to

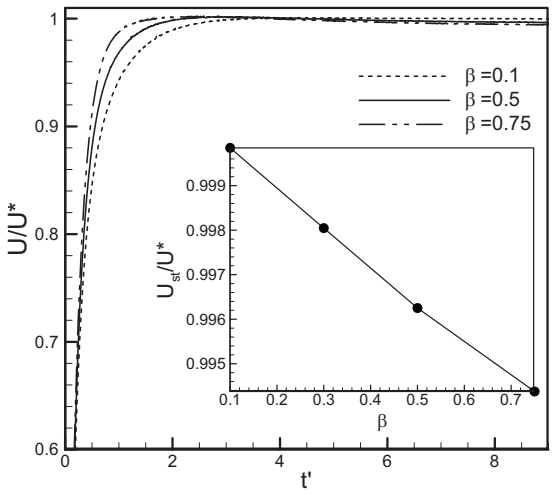

FIG. 6. Effect of β on the velocity of a falling viscoelastic drop for Ca=0.3, De=1.52, and Fr=0.34. Inset shows the steady state velocity.

De increase. The inset shows that the steady state velocity varies linearly with β. We note that the velocity decrease due to viscoelasticity in Figs. 5 and 6 are small. Furthermore, as we increase the Deborah number further, the drop becomes unstable. We will discuss unstable cases below to show that the velocity reduces drastically for them. Previous experiment[15] (Fig. 6 in that reference) showed significant change in velocity from the Newtonian value for a very high viscosity ratio drop (λ_μ=50), and only above De=20. High viscosity ratio and high Deborah cases show long transient and requires very small time steps for numerical simulation. Preliminary numerical simulation indicates that at higher viscosity ratios, a viscoelastic drop remains stable for higher Deborah numbers experiencing at the same time further decrease in its falling velocity. Here, we restrict ourselves to a viscosity matched system. (Note also that an analytical result plotted using a perturbation method with a third order fluid in the same figure of the above reference has a numerical error resulting in underprediction of the velocity; the corrected analytical prediction matches well with the simulation.) We also point out that Oldroyd-B is a model constitutive equation which is useful for providing qualitative understanding of a phenomenon, but might not be appropriate for accurately describing the response of any real fluid.

We plot the steady state cross-sectional length L_{cross}/a (maximum distance from the vertical axis of symmetry) in Fig. 7 that shows an increase with De consistent with the lower terminal velocity seen in Fig. 5. We note that the change in velocity or the cross-sectional dimension is small with drop viscoelasticity. However, as noted before a dimple forms at the rear end. We plot in the same figure (Fig. 7) the distance of the dimple tip from the drop's center of mass b/a. The dimple progressively advances toward the drop center with increasing De. In Fig. 8, several steady drop shapes for various combinations of Deborah and capillary numbers are shown. Higher Deborah number leads to more pronounced dimple. Lower capillary number inhibits large

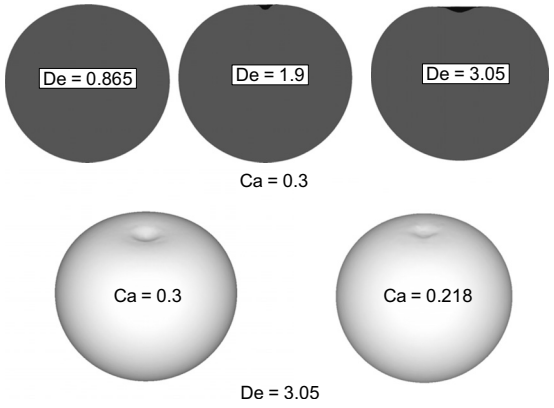

FIG. 8. Steady state shapes of falling viscoelastic drops at $Fr=0.34$.

curvature, and therefore leads to wider and shallower dimple. For the larger capillary number, we see a narrower and deeper dimple.

In Fig. 9, we plot velocity vectors for a viscoelastic drop (with respect to the drop) for $Ca=0.61$ and $De=1.52$. We observe that they are not very different from those for a Newtonian drop (Fig. 4), the only difference being due to the dimple. To further investigate the effects of elasticity, T^p_{zz} on the central plane of the drop is also plotted in Fig. 9. T^p_{zz} has much higher values than the other stress components (T^p_{xx}, T^p_{yy}, T^p_{xy}, etc. are not shown here). T^p_{zz} is concentrated at the rear end of the drop just inside the interface which coincides with the dimple region suggesting that T^p_{zz} is the main cause for the formation of the dimple.

B. Mechanism of dimple formation

Formation of the dimple at the rear end of the drop is similar in nature to the blunt ends of a viscoelastic drop in an extensional flow[26] where the flow in the vicinity of the drop tip is extensional and the drop pulls itself toward the center. The falling drop experiences uniaxial contraction in the front, and uniaxial extension in the rear end. Near the front, the stress is higher in the extensional flow parallel to the drop surface. In contrast, extension normal to the interface at the rear end pulls the interface inward. To gain insight into the underlying physics, we resort to an approximate analysis of the problem. We assume that for small amount of viscoelasticity, the drop shape remains almost spherical as indeed we

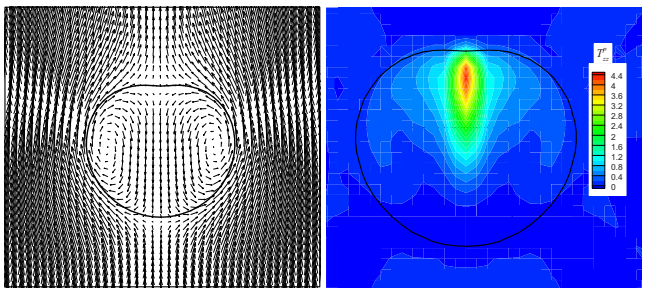

FIG. 9. (Color online) Velocity vectors (left) in a falling viscoelastic drop for $Ca=0.61$, $De=1.52$, and $Fr=0.34$, and contour of viscoelastic stress T^p_{zz} (right).

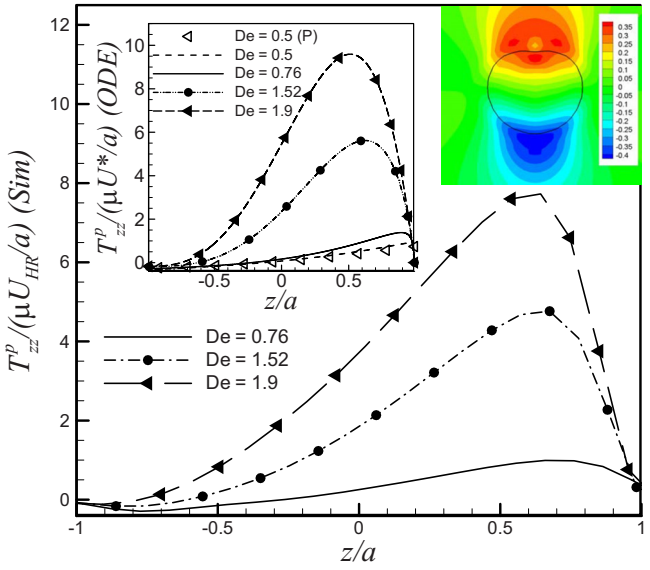

FIG. 10. (Color online) T^p_{zz} along the axis of symmetry for different Deborah numbers from simulation and one-dimensional model (inset) for $Ca=0.61$ and $Fr=0.34$. Top right inset shows the contours of dw/dz for $De=1.52$. In the left inset the curve (P) corresponds to the perturbative solution.

saw above, and the velocity field can be approximated by that from the Newtonian case, i.e., the Hadamard–Rybczynski velocity field. One can then use Oldroyd-B equation to find the stress component T^p_{zz} along the axis of symmetry where velocity field has only the vertical component w

$$w\frac{dT^p_{zz}}{dz}+\frac{T^p_{zz}}{\lambda}=\left(\frac{2\mu_p}{\lambda}+2T^p_{zz}\right)\left(\frac{dw}{dz}\right). \tag{2}$$

Using the velocity field (in a coordinate system fixed to the center of the drop)

$$w=-\frac{U_{\mathrm{HR}}}{2(1+\lambda_\mu)}\left(1-\frac{z^2}{a^2}\right) \tag{3}$$

one obtains

$$-(U_{\mathrm{HR}}/4)\frac{dT^p_{zz}}{dz}\left(1-\frac{z^2}{a^2}\right)+T^p_{zz}\left(\frac{1}{\lambda}-\frac{U_{\mathrm{HR}}}{a^2}z\right)=\left(\frac{U_{\mathrm{HR}}\mu_p}{\lambda a^2}\right)z. \tag{4}$$

Note that because we found that the other stress components are much smaller, they are neglected in this analysis. One can actually solve Eq. (4) to find T^p_{zz} along the axis of symmetry

$$T^p_{zz}(z)=e^{\int^z q(z')dz'}\left[\int^z h(z'')e^{-\int^{z''}q(\xi)d\xi}dz''+\mathrm{const}\right], \tag{5}$$

$$q(z)=\frac{4(a^2-U_{\mathrm{HR}}z\lambda)}{U_{\mathrm{HR}}\lambda(a^2-z^2)},\quad h(z)=-\frac{4\mu_p z}{\lambda(a^2-z^2)}.$$

The plotted T^p_{zz} in Fig. 10 both from the simulation and the above Eq. (4) (inset) are qualitatively similar. The similarity indicates that the approximate analysis captures the essential dynamics. We therefore can use the simpler Eqs. (2) and (4) to understand it. Both simulation and the model show that with increasing Deborah number (i.e., increasing λ), the

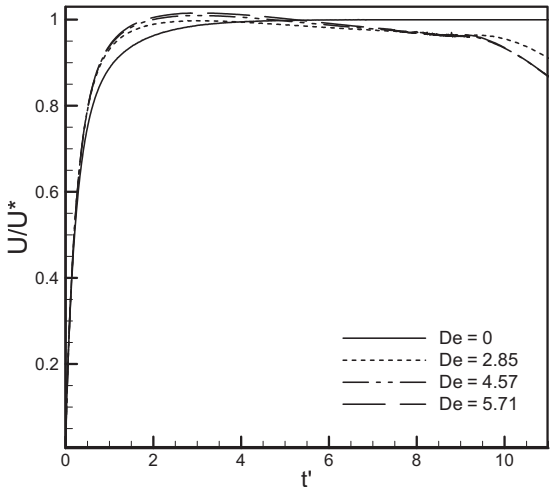

FIG. 11. Effect of Deborah number on the velocity of an unstable drop for $Ca=2.28$ and $Fr=0.42$.

stress increases dramatically at the location of maximum near the rear end, where the dimple appears. The location of the maximum shifts toward the drop center with increasing viscoelasticity indicating the growing inward pull and correspondingly a more pronounced dimple. Note that in absence of viscoelasticity ($De=0$), the stress in Eq. (2) satisfies the Newtonian equation $T^p_{zz}=2\mu_p dw/dz$. From Eq. (3), one sees that $dw/dz\sim z$ and therefore antisymmetric across the center plane ($z=0$) of the axes fixed to the drop [note T^0_{zz} below in Eq. (7) below]. Indeed the simulated solution indicates dw/dz (for $Ca=0.61$ and $De=1.52$) very similar to such an antisymmetric field (inset of Fig. 10). The analytical solution (5) does not lend to easy understanding. To further understand the increase of stress near the rear end, we write Eq. (4) in a nondimensional form (use $\mu U_{\mathrm{HR}}/a$ for scaling stresses)

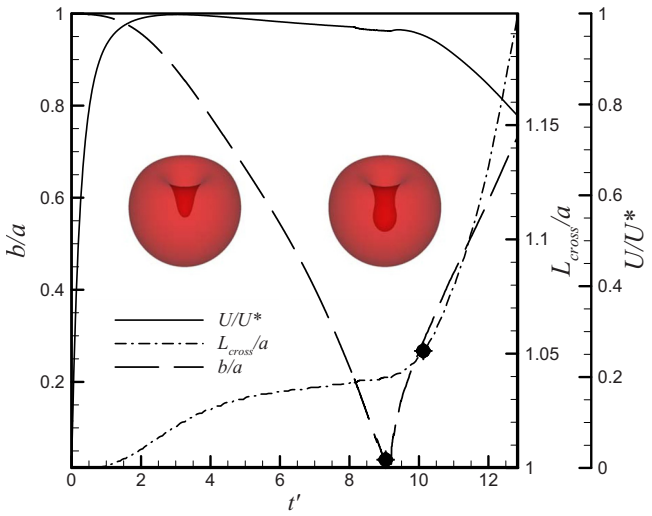

FIG. 12. (Color online) Cross-sectional length L_{cross}, dimple distance b, and velocity of an unstable drop for $Ca=2.28$, $De=2.85$, and $Fr=0.42$. Drop shapes are also shown at instants marked.

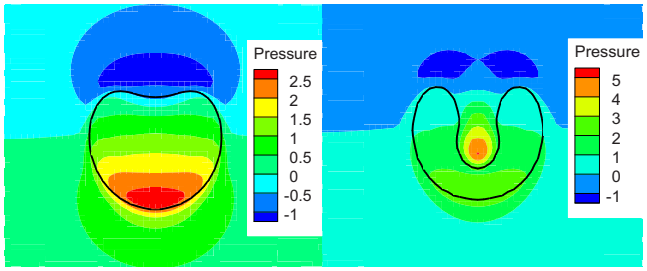

FIG. 13. (Color online) Pressure contours at nondimensional times 4.57 and 10.28 for the same case as in Fig. 11.

$$-\frac{De}{4}(1-z^2)\frac{dT^p_{zz}}{dz}+T^p_{zz}-DezT^p_{zz}=\beta z. \tag{6}$$

Using a regular perturbation method one obtains

$$T^p_{zz}=T^0_{zz}+DeT^1_{zz},$$

$$T^0_{zz}=\beta z, \tag{7}$$

$$T^1_{zz}=\frac{\beta}{4}(3z^2+1).$$

The zeroth order solution is the Newtonian stress. The order De solution increases stress at the rear end ($z=1$), and reduces its magnitude at the forward end ($z=-1$). This solution plotted for the lowest Deborah number $De=0.5$ (marked as P in the inset of Fig. 10) shows excellent match with the model solution. The increased stress at the rear end causes the dimple. This analysis is only meant to show the asymmetric growth of the viscoelastic stress along the drop axis based on the Newtonian velocity field. Note that the Newtonian drop remains spherical, and the corresponding velocity field (3) is independent of capillary number. As the capillary number or the viscoelasticity that causes the dimple is further increased,

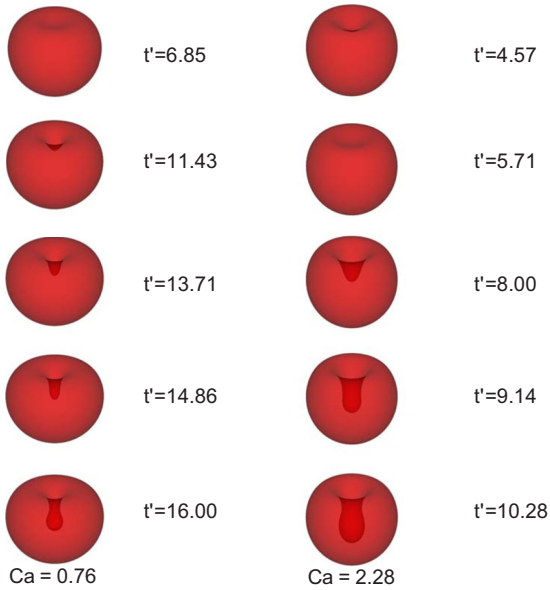

FIG. 14. (Color online) Transient evolution for two sets of capillary numbers and $Fr=0.42$.

the drop becomes unstable. Our code cannot handle topological change and therefore, cannot simulate torus formation. However, it can simulate the phenomenon leading to it.

C. Unstable cases

When the surface tension becomes unable to overcome the dimple forming viscoelastic stresses, the dimple grows unbounded. Recent experimental investigation of the problem[15] saw this phenomenon with increasing drop size (which is equivalent to increasing capillary number as well as increasing Deborah number, the latter, because increasing radius increases velocity), in that the dimple grows to reach the other side of the drop forming a doughnutlike structure. The velocity plotted for different De values for a fixed capillary number (Fig. 11) shows that, for these unstable cases, velocity continues to decrease, and after a particular time instant, it changes slope marking even more rapid decrease. We investigate this further for one case ($De=2.85$) from Fig. 11, where drop profiles at two close time instants show that the sudden change (around $t'=9$) coincides with the dimple developing a small globular shape at the bottom (Fig. 12). It makes the drop to widen even more making the dimensionless cross-sectional length (L_{cross}/a) also experience a sudden increase around the same time. Note that b/a plot shows that the distance of the tip from the center of mass becomes zero and starts growing again (i.e., the center of mass goes out of the drop) around the same time.

In Fig. 13, we plot the pressure field at two time instants before and after the shape change in dimple takes place for the same case studied in Fig. 12. Initially the highest pressure is at the front bulbous end of the drop. After the dimple itself develops a globular end, the highest pressure occurs there because of the smaller radius of curvature. The globule pushes the drop boundary radially outward causing an increased cross-sectional length (Fig. 12). Finally, it leads to the formation of torus.[15] Note that torus formation has also been noted for Newtonian fluids,[4,27] especially when the surface tension has a very small value.[28] However, here torus formation is driven by the viscoelastic stresses analyzed before in Sec. IV B. In Fig. 14, evolution of unstable drop shape for two capillary numbers at the same Deborah number and $Fr=0.42$ is shown. Note that the smaller capillary number leads to a more pronounced globular shape at the end of the dimple; the larger interfacial tension force leads to this spherical end. In contrast, the larger capillary number tends to take a more cylindrical shape, which eventually touches the other end to from the torus.

In Fig. 15, we investigate the drop's stability curve as a function of capillary and Deborah numbers. However, finding the precise values of the two numbers, where drop transitions from a stable to an unstable case is difficult to determine numerically—near transition the very nature of the problem makes its behavior susceptible to large changes depending on precise numerical implementation such as domain size, spatial resolution, and time stepping. However, careful simulation can provide a qualitative idea about the transition. In Fig. 15, for each capillary number (plotted as $k=Ca^{-1}$), we simulate cases with increasing Deborah number

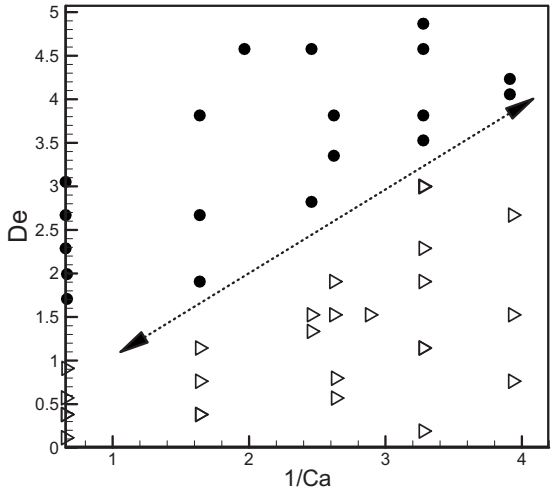

FIG. 15. Phase plot of stability for $Fr=0.34$ simulated cases (triangles are stable and circles are unstable).

to find stable and unstable cases. Near the transition the simulations are checked with higher resolution. There is a zone of parameters near the transition, where it proves difficult to determine whether the case is stable or unstable as it has a very slow time scale of development. We only show the cases where we are certain about the final nature of the solution. The line drawn approximately separates the stable from the unstable cases. As expected, increasing k (decreasing capillary number) increases the critical Deborah number—higher surface tension requires higher stronger viscoelastic stresses to makes the drop unstable. One notes an approximately linear relation $De_{\text{critical}} \sim 1/Ca$.

V. CONCLUSION

We have employed front-tracking finite difference method to investigate the settling of a viscoelastic drop heavier than the surrounding media. Unlike the spherical shape of a Newtonian drop, a viscoelastic drop departs from its spherical shape due to the viscoelastic stresses at its rear end. The polymeric stress T^p_{zz}, which is caused by the uniaxial extension at that end, pulls the interface inward flattening and finally forming a dimple as the De is increased. We performed an approximate analysis of the problem using the velocity field for a Newtonian drop to establish that with increasing viscoelasticity this stress component experiences a large increase. At the same time, its maximum point progressively deviates away from the rear end toward the center. The viscoelastic stress acts against the surface tension which tries to retain the spherical shape. As the drop deforms from the spherical shape, the settling velocity decreases, decrease being monotonic with De, Ca, and β (the polymeric part of the viscosity).

Further increase in viscoelasticity or decrease in surface tension makes the drop unstable with continuous change in shape. The dimple starts to grow eventually touching the other side of the drop creating a toroidal shape. But before that, the dimple develops a globular shape, which coincides with a sudden increase in drop cross-section and concomitant decrease in drop velocity. A phase plot in the space of De

and Ca shows that the critical Deborah number, that separates the stable drops below it from the unstable one above, approximately follows a scaling $De_{\text{critical}} \sim Ca^{-1}$.

ACKNOWLEDGMENTS

K.S. acknowledges financial support from NSF Grant No. CBET-0625599. The authors thank Michael Sostarecz for a discussion about the analytical results in Ref. 15, and William R. Schowalter for pointing out an error in the one-dimensional model computation. S.M. acknowledges helpful discussion with Nishith Aggarwal.

[1] J. Hadamard, "Mouvement permanent lent d'une sphere liquide et visqueuse dans un liquide visqueux," C. R. Hebd. Seances Acad. Sci. **152**, 1735 (1911).
[2] W. Rybczynski, "Uber die fortschreitende Bewegung einer flüssigen Kugel in einem zähen Medium," Bull. Int. Acad. Sci. Cracovie **A**, 40 (1911).
[3] T. D. Taylor and A. Acrivos, "On the deformation and drag of a falling viscous drop at low Reynolds number," J. Fluid Mech. **18**, 466 (1964).
[4] M. Kojima, E. J. Hinch, and A. Acrivos, "The formation and expansion of a toroidal drop moving in a viscous fluid," Phys. Fluids **27**, 19 (1984).
[5] C. J. Koh and L. G. Leal, "The stability of drop shapes for translation at zero Reynolds number through a quiescent fluid," Phys. Fluids A **1**, 1309 (1989).
[6] R. P. Chhabra, *Bubbles, Drops, and Particles in Non-Newtonian Fluids*, 2nd ed. (CRC, Boca Raton, 2007).
[7] R. A. Brown, M. J. Szady, P. J. Northey, and R. C. Armstrong, "On the numerical stability of mixed finite-element methods for viscoelastic flows governed by differential constitutive equations," Theor. Comput. Fluid Dyn. **5**, 77 (1993).
[8] M. J. Szady, T. R. Salamon, A. W. Liu, D. E. Bornside, R. C. Armstrong, and R. A. Brown, "A new mixed finite-element method for viscoelastic flows governed by differential constitutive equations," J. Non-Newtonian Fluid Mech. **59**, 215 (1995).
[9] O. Hassager, "Negative wake behind bubbles in non-Newtonian liquids," Nature (London) **279**, 402 (1979).
[10] W. Philippoff, "Viscosity characteristics of rubber solution," Rubber Chem. Technol. **10**, 76 (1937).
[11] D. Rodrigue, D. De Kee, and C. F. Chan Man Fong, "Bubble velocities: Further developments on the jump discontinuity," J. Non-Newtonian Fluid Mech. **79**, 45 (1998).
[12] M. Astarita and G. Apuzzo, "Motion of gas bubbles in non-Newtonian liquids," AIChE J. **11**, 815 (1965).
[13] S. B. Pillapakkam, P. Singh, D. Blackmore, and N. Aubry, "Transient and steady state of a rising bubble in a viscoelastic fluid," J. Fluid Mech. **589**, 215 (2007).
[14] M. G. Wagner and J. C. Slattery, "Slow flow of a non-Newtonian fluid past a droplet," AIChE J. **17**, 1198 (1971).
[15] M. C. Sostarecz and A. Belmonte, "Motion and shape of a viscoelastic drop falling through a viscous fluid," J. Fluid Mech. **497**, 235 (2003).
[16] R. You, H. Haj-Hariri, and A. Borhan, "Confined drop motion in viscoelastic two-phase systems," Phys. Fluids **21**, 013102 (2009).
[17] R. You, A. Borhan, and H. Haj-Hariri, "A finite volume formulation for simulating drop motion in a viscoelastic two-phase system," J. Non-Newtonian Fluid Mech. **153**, 109 (2008).
[18] K. Sarkar and W. R. Schowalter, "Deformation of a two-dimensional drop at nonzero Reynolds number in time-periodic extensional flows: Numerical simulation," J. Fluid Mech. **436**, 177 (2001).
[19] N. Aggarwal and K. Sarkar, "Deformation and breakup of a viscoelastic drop in a Newtonian matrix under steady shear," J. Fluid Mech. **584**, 1 (2007).
[20] N. Aggarwal and K. Sarkar, "Effects of matrix viscoelasticity on viscous and viscoelastic drop deformation in a shear flow," J. Fluid Mech. **601**, 63 (2008).
[21] N. Aggarwal and K. Sarkar, "Rheology of an emulsion of viscoelastic drops in steady shear," J. Non-Newtonian Fluid Mech. **150**, 19 (2008).
[22] S. Mukherjee and K. Sarkar, "Effects of viscosity ratio on deformation of a viscoelastic drop in a Newtonian matrix under steady shear," J. Non-Newtonian Fluid Mech. **160**, 104 (2009).
[23] S. Mukherjee and K. Sarkar, "Effects of viscoelasticity on the retraction of a sheared drop," J. Non-Newtonian Fluid Mech. **165**, 340 (2010).
[24] S. O. Unverdi and G. Tryggvason, "A front-tracking method for viscous, incompressible multifluid flows," J. Comput. Phys. **100**, 25 (1992).
[25] K. Sarkar and W. R. Schowalter, "Deformation of a two-dimensional viscoelastic drop at nonzero Reynolds number in time-periodic extensional flows," J. Non-Newtonian Fluid Mech. **95**, 315 (2000).
[26] A. S. Hsu and L. G. Leal, "Deformation of a viscoelastic drop in planar extensional flows of a Newtonian fluid," J. Non-Newtonian Fluid Mech. **160**, 176 (2009).
[27] G. Machu, W. Meile, L. C. Nitsche, and U. Schaflinger, "Coalescence, torus formation, and breakup of sedimenting drops: Experiments and computer simulations," J. Fluid Mech. **447**, 299 (2001).
[28] N. Baumann, D. D. Joseph, P. Mohr, and Y. Renardy, "Vortex rings of one fluid in another in free-fall," Phys. Fluids A **4**, 567 (1992).